Journal of Solid State Chemistry 183 (2010) 1448–1456

Contents lists available at ScienceDirect

Journal of Solid State Chemistry

journal homepage: www.elsevier.com/locate/jssc

Synthesis and textural evolution of alumina particles with mesoporous structures

Xun Liu, Tianyou Peng *, Jinchun Yao, Hongjin Lv, Cheng Huang

College of Chemistry and Molecular Science, Wuhan University, Wuhan 430072, PR China

ARTICLE INFO

Article history:
Received 8 February 2010
Received in revised form
31 March 2010
Accepted 13 April 2010
Available online 22 April 2010

Keyword:
Nanostructure
Alumina
Chemical synthesis
Mesostructure

ABSTRACT

Alumina particles with mesostructures were synthesized through a chemical precipitation method by using different inorganic aluminum salts followed by a heterogeneous azeotropic distillation and calcination process. The obtained mesoporous γ-alumina particles were systematically characterized by the X-ray diffraction, transmission electron microscopy and nitrogen adsorption–desorption measurement. Effects of the aluminum salt counter anion, pH value and the azeotropic distillation process on the structural or textural evolution of alumina particles were investigated. It is found that Cl^- in the reaction solution can restrain the textural evolution of the resultant precipitates into two-dimensional crystallized pseudoboehmite lamellae during the heterogeneous azeotropic distillation, and then transformed into γ-Al_2O_3 particles with mesostructures after further calcination at 1173 K, whereas coexisting SO_4^{2-} can promote above morphology evolution and then transformed into γ-Al_2O_3 nanofibers after calcination at 1173 K. Moreover nearly all materials retain relatively high specific surface areas larger than 100 $m^2 g^{-1}$ even after calcinations at 1173 K.

1. Introduction

Discovery of silica-based mesoporous molecular sieves (M41S family) in 1992 revealed exciting possibilities for new types of molecular sieve with significantly larger pore and narrower pore size distribution in comparison with zeolites [1,2]. Thereafter, various synthesis methods have been proposed to prepare various inorganic mesoporous materials with controllable porosity and high thermal stability. As an important engineering material, mesoporous alumina (Al_2O_3) has been extensively used in the fields of catalysis, adsorption and separation due to its favorable combination of textural properties such as specific surface area, pore volume and pore size distribution [3–5].

Syntheses of ordered mesoporous Al_2O_3 with narrow pore size distribution have been actualized through traditional cationic, anionic, or neutral surfactant-mediated templating routes [6–11], and those surfactants as structure-directing agents have been applied to direct the formation of mesophases and to control the pore size and shape on the bases of electrostatic and hydrogen bonding interactions. Most of these synthetic processes usually stemmed from aluminum alkoxides. Pseudoboehmite has also been used as starting material for the fabrication of mesoporous γ-Al_2O_3 in the presence of different hydrocarboxylic acids [12]. Moreover alumina materials with different morphologies, such as nanotube, nanorod, nanofiber, nanoplate and nanosheet have been fabricated via a template-free solvothermal process by adjusting the ratio and composition of the reaction solutions [13]. The raw materials used above, however, were usually expensive alkoxides, pseudoboehmite or environmentally hazardous organic solvent.

The first synthesis of alumina-based mesoporous material in aqueous solution has been reported by Huo et al. [14]. Lamellar, thermally unstable mesophases have been obtained from an aqueous media involving Al^{3+} and anionic surfactants such as alkylsulfonates or phosphates, whereas vermicular mesoporous alumina with specific surface area of 250 ~ 300 $m^2 g^{-1}$ has been fabricated by using cheap materials such as inorganic aluminum salts and long-chain, inexpensive nonionic surfactant (polyethylene glycol) [15]. The formation mechanism of mesoporous particles has been attributed to a self-assembly process of inorganic precursor [15]. This explanation was based on the function of precipitator (ammonium bicarbonate), which can slower the precipitate reaction rate. The inorganic precursors were gradually precipitated and piled up in a proper rate, and then formed the mesoporous structures under an appropriate reaction conditions such as 343 K reaction temperature [15].

Similarly, mesoporous alumina with specific surface area of 342 $m^2 g^{-1}$ and narrow pore size distribution centered at 3.9 nm has been fabricated based on a novel double hydrolyses of Al^{3+} and AlO_2^- in the presence of P123 [16]. It has been found that the pore structures of above mesoporous alumina were easy to crack during the drying process due to the high surface tension of water. One way to overcome this shortcoming is to replace the water absorbed on the surfaces of precipitated precursor by using

* Corresponding author: Fax: +86 27 68752237.
E-mail addresses: typeng@whu.edu.cn, typeng2001@tom.com (T. Peng).

0022-4596/$ - see front matter © 2010 Elsevier Inc. All rights reserved.
doi:10.1016/j.jssc.2010.04.020

organic solvent such as methanol to decrease the surface tension [6]. Supercritical drying process, which benefits from the lower surface tension near the solvent's supercritical point [17–19], has been utilized to synthesize mesoporous Al_2O_3 with pore diameter of 2–20 nm by using sodium aluminate as starting material [20]. It has been found that the aging temperature of 363 K, aging time of 3 h and methanol replacing were enough to form mesoporous Al_2O_3 with specific surface area of 367 $m^2 g^{-1}$. Recently, γ-Al_2O_3 nanoparticles with porous structures have been prepared by a co-precipitation/digestion method [21]. During the precipitation process, sodium carbonate was used as a precipitant and, co-precipitation/digestion was carried out simultaneously at 343 K for 3 h. The OH^- *in situ* produced by the hydrolysis of carbonate in aqueous medium could promote the precipitation process, and the porosity was derived from the pileup among the nanoparticles. It was difficult to control the morphology and pore diameter of above alumina because of its instability due to the faint interaction between the surfactant and precursor as well as the fast hydrolysis. Therefore, it is necessary to establish a set of convenient and inexpensive synthetic technique for the industrial preparation of mesoporous Al_2O_3 with controllable morphology, narrow pore size distribution and excellent thermal stability.

Recently, γ-Al_2O_3 nanofibers with ca. 3–5 nm thick and 50–150 nm long have been prepared via a precipitation process [22]. It was found that the resulting spherical aluminum hydrate precipitates are evolved into two-dimensional crystallized pseudoboehmite lamellae after the heterogeneous azeotropic distillation, and then transformed into γ-Al_2O_3 nanofibers after further calcination at 1173 K. However, the crystal phase and morphology transformations can only be observed in the situation of an $NH_4Al(SO_4)_2$ solution with near neutral condition, whereas precipitate derived from the acidic reaction solution shows granular alumina with mesostructures, which is completely different from the above mentioned phenomena [22]. The differences in the morphologies and phase transformation can be ascribed to the directing function of PEG and the counter anions in the reaction solution with different acidic conditions [23].

Herein, a chemical precipitation process in the presence of polyethylene glycol (PEG) was applied to prepare the precipitated precursor, which was dehydrated through a heterogeneous azeotropic distillation process with *n*-butanol and calcined to synthesize γ-Al_2O_3 particles with mesostructures. The whole precipitation process was conducted in an aqueous media at room temperature using ammonium bicarbonate and different inorganic aluminum salts as starting materials. Experimental results show that alumina particles with intraparticle or interparticle porous structures can be obtained by optimizing the experimental conditions. The effects of counter anion, pH value, surfactant PEG and the azeotropic distillation process on the textural and structural evolutions of alumina particles were investigated in detail. Moreover the formation mechanism of mesoporous γ-Al_2O_3 particles was also discussed.

2. Experimental section

2.1. Materials

All chemicals used are analytical reagents. $AlCl_3 \cdot 6H_2O$ or $NH_4Al(SO_4)_2 \cdot 12H_2O$ (Sinopharm Chemical Reagent Co. Ltd.) are used as aluminum sources. Polyethylene glycol molecules (PEG 2000 and PEG 400, Sinopharm Chemical Reagent Co. Ltd.) have a general formula as $H(OCH_2–CH_2)_nOH$, and their average molecular weights are about 1900–2200 and 380–420 for PEG 2000 and PEG 400, respectively. Ammonium bicarbonate, ammonia, nitric acid, *n*-butanol, anhydrous ethanol (Shanghai Shengbo Chemical Industry Co. Ltd.) were used without further purification.

2.2. Preparation

A 0.4 mol L^{-1} NH_4HCO_3 aqueous solution containing 8.8 wt% PEG 2000 was obtained by dissolving 3.2 g NH_4HCO_3 and 10.0 g PEG 2000 in 100 mL of distilled water under magnetic stirring. Two kinds of 0.4 mol L^{-1} aluminum salt solutions containing PEG 400 were prepared by dissolving 5.0 g PEG 400 and 9.1 g $NH_4Al(SO_4)_2 \cdot 12H_2O$ or 4.8 g $AlCl_3 \cdot 6H_2O$ in 50 mL of distilled water under magnetic stirring, respectively.

A 50 mL of the above $NH_4Al(SO_4)_2$ solution was added dropwise into 100 mL of NH_4HCO_3 solution under vigorous stirring. And the terminal pH value of the reaction mixture was adjusted by nitric acid and/or ammonia (6.4–7.2 mol L^{-1}) to pH 5.00 or 7.00–8.00, respectively. The reaction mixture was further stirred for about 0.5 h, and then aged for another 2 h without stirring. The resulting white precipitate was recovered by centrifugation and washed with distilled water and anhydrous ethanol several times to obtain the as-synthesized precursor. The above products derived from $NH_4Al(SO_4)_2$ were marked as PS1-5 (pH 5.00) and PS1-7 (pH 7.00–8.00), respectively. For comparison, $AlCl_3$ solution was also used as an aluminum source to prepare the precursor through the same procedure, and the resultant products were marked as PC1-5 (pH 5.00) and PC1-7 (pH 7.00–8.00), respectively.

The as-synthesized precursor was dehydrated by a heterogeneous azeotropic distillation process as follows [22]: The precursor was transferred into a rockered flask containing 200 mL of *n*-butanol, and then the slurry was heated to 365–367 K to evaporate the water–butanol azeotrope under stirring continuously. Once the temperature of the vaporized fraction reached 390 K (*b.p.* of *n*-butanol), the slurry was kept on refluxing for 2 h. The remaining *n*-butanol was removed through under pressure distillation to obtain loose powders, and these dehydrated products of PS1-5, PS1-7, PC1-5 and PC1-7 were denoted as PS2-5, PS2-7, PC2-5 and PC2-7, respectively. The dehydrated powders were further heated in air at a heating rate of 10 K min^{-1} and then calcined at target temperature for 2 h to obtain the final products. The products derived from an $NH_4Al(SO_4)_2$ and $AlCl_3$ solution were denoted as PS3-X-T and PC3-X-T, respectively. Here, *X* is the pH value of the reaction mixture, and T is the calcination temperature. For example, PS3-5-1173 denotes the product derived from $NH_4Al(SO_4)_2$ at pH 5.00, followed by distillation process and calcined at 1173 K.

2.3. Characterization

The crystal phase compositions were identified by a XRD-6000 diffractometer (Shimadzu, Japan) using Cu Kα1 radiation ($\lambda = 1.5406$ Å) and a fixed power source (40 kV, 40 mA). A continuous scan mode was used to collect 2θ in 20–70° with the scanning rate of 4°(θ) min^{-1}. The morphology of the sample was observed on a JEOL 2010 transmission electron microscope (TEM, Japan Electronics), the powder sample was deposited onto a copper mesh grid coated with a carbon film. Liquid N_2 adsorption–desorption data was obtained by using an ASAP 2020 apparatus (Micromeritics). The specific surface area was calculated by the Brunauer–Emmett–Teller (BET) equation and pore size distribution was determined using the desorption branch based on the Barrett–Joyner–Helenda (BJH) model.

3. Results and discussion

3.1. Effects of the reaction conditions on the morphologies of the products

Typical TEM images of four kinds of calcined product derived from $NH_4Al(SO_4)_2$ or $AlCl_3$ solutions with different pH values are shown in Fig. 1. As can be seen, PC3-5-1173 derived from $AlCl_3$ solution with pH 5.00 shows quasispherical nanoparticle with secondary particle diameters in the range 50∼120 nm and loose porous structures, which is made up of pileup pores of tiny primary particles with particle sizes of 7∼14 nm (Fig. 1a); and PC3-7-1173 derived from an $AlCl_3$ solution with pH 7.00–8.00 shows porous particles with obvious interlocked surfaces and intraparticle pores (Fig. 1b), the particle size distribution is in the range 30∼100 nm. Whereas quasispherical particles (Fig. 1c) with close-knit intraparticle porous structures and more regular shapes (particle size distribution in the range 60∼90 nm) were observed in PS3-5-1173 derived from an $NH_4Al(SO_4)_2$ solution with pH 5.00, and PS3-7-1173 derived from an $NH_4Al(SO_4)_2$ solution with pH 7.00–8.00 shows nanofibers with ca. 3–5 nm and 50–150 nm longer fibrous nanoparticles (Fig. 1d) as described in our previous paper [22]. All products were synthesized via the same procedure, except for different pH values and aluminum salt counter anions. Therefore, the effects of counter anion, pH value and the distillation process on the structural or textural evolution of alumina particles were further investigated in the present work.

Correlative TEM observations for various precipitated precursors are performed to further investigate the formation mechanism of the γ-Al_2O_3 particles with porous structures. As shown in Fig. 2, the precipitate (PC1-5) derived from an $AlCl_3$ solution with pH 5.00 is loose porous structures made up of pileup pores of primary particles with particle sizes of 5∼9 nm (Fig. 2a), which is similar to its relevant calcined product (Fig. 1a), while the PC1-7 are spherical particles (Fig. 2b) with obvious intraparticle porous structures, which show more smooth surfaces and smaller particle size than PC1-5. As for the precipitates derived from an $NH_4Al(SO_4)_2$ solution, the peripheries of product PS1-5 particles show merged and smooth surfaces, which contain interparticle porous structures (Fig. 2c) consisted of much smaller primary particles in comparison with PC1-7; while the precipitate (PS1-7) consists of amorphous spherical floccules (Fig. 2d) with particle sizes in the range 25∼45 nm, and this precipitate has much denser and irregular particle morphologies than the product PC1-7, it is also different from the calcined product PS3-7-1173 (Fig. 1d), the corresponding morphology transformation during the post-treatment and calcination processes has been discussed in our previous paper [22].

Fig. 3 shows TEM images of four kinds of intermediate after the heterogeneous azeotropic distillation process. As can be seen, PC2-5 shows particles morphology consisted of loose accumulation of primary particles (Fig. 3a), and PC2-7 has a disorderly morphology with obvious intraparticle pores and interlocked particle surfaces (Fig. 3b). Generally, PC2-5 and PC2-7 show quasispherical structures similar to those of the relative precipitate PC1-5 (Fig. 2a) and calcined product PC3-7-1173 (Fig. 1b), indicating that limited reconstructions were occurred in these precipitates during the post-treatment processes. However, PS2-5 (Fig. 3c) shows some differences from those of PS1-5 and PS3-5-1173, it consists of an accumulation with more compact aggregation, indicating that the microstructures have changed during the distillation and calcination processes, whereas the amorphous floccus PS2-7 transformed into lamellar structures (Fig. 3d) [22].

On the bases of above TEM observations, it could be concluded that the differences in the morphology are related to the counter anions, the existing form of PEG molecule in the reaction solutions with different acidities. Firstly, the co-existing Cl^- would result in γ-Al_2O_3 particles with a porous structure, the pileup pores can be obtained from an acidic reaction solution, and intraparticle porous structures would be formed under a near neutral reaction solution; Secondly, introducing SO_4^{2-} would lead to the transformation of amorphous floccus obtained in the near neutral solution into lamellar pseudoboehmite, and then to γ-Al_2O_3 nanofibers

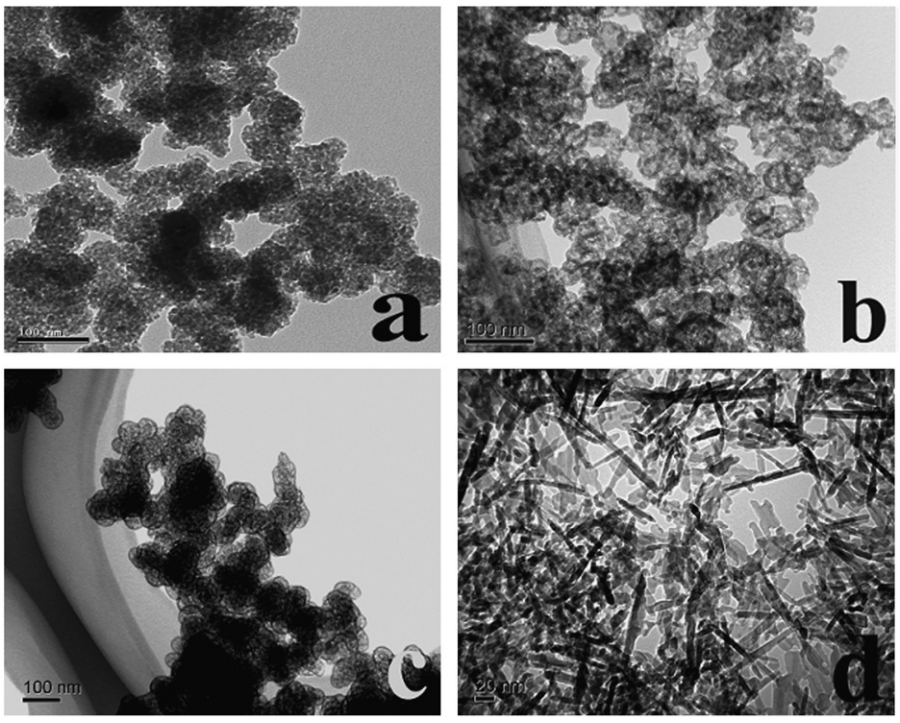

Fig. 1. TEM images of various calcined products derived from different reaction conditions: (a) PC3-5-1173, (b) PC3-7-1173, (c) PS3-5-1173 [22] and (d) PS3-7-1173 [22].

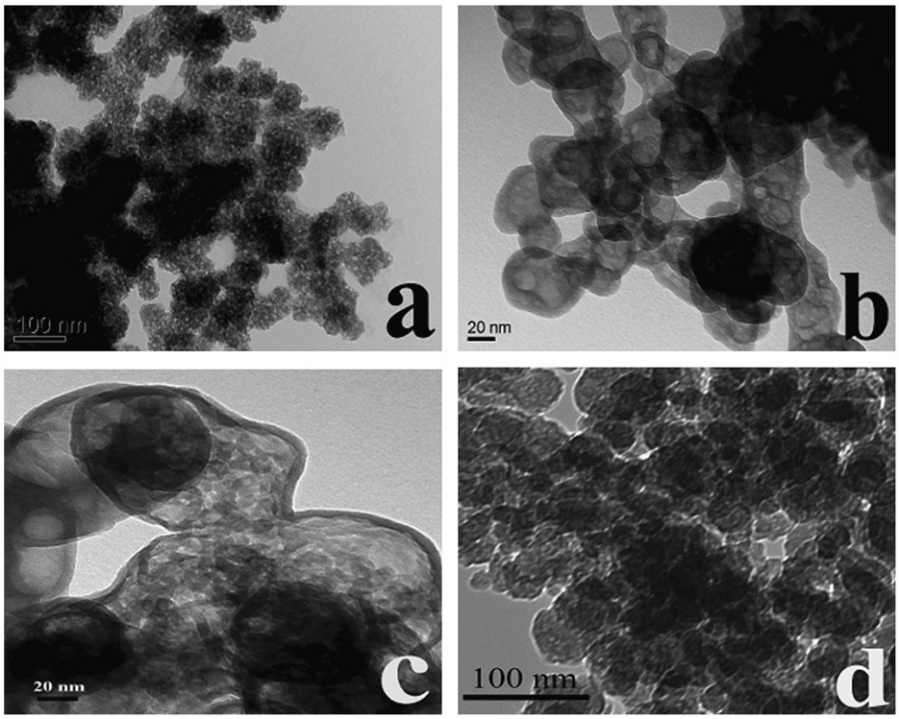

Fig. 2. TEM images of various precipitates derived from different reaction conditions: (a): PC1-5; (b): PC1-7; (c): PS1-5 and (d): PS1-7.

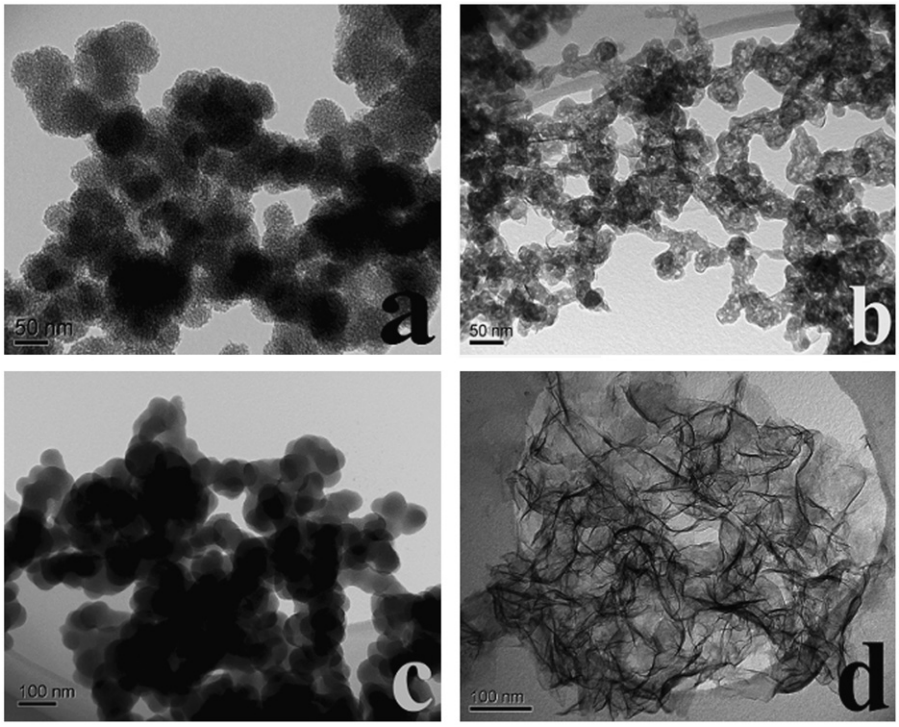

Fig. 3. TEM images of various precursors derived from different reaction conditions after a heterogeneous azeotropic distillation process: (a) PC2-5, (b) PC2-7, (c) PS2-5 and (d) PS2-7.

after calcination [22]; and γ-Al_2O_3 particles with intraparticle porous structures can be obtained from an acidic reaction solution. Thirdly, γ-Al_2O_3 particles synthesized with $AlCl_3$ or $NH_4Al(SO_4)_2$ in an acidic solution still have some differences in the morphology due to effects of anions during the precipitation and post-treatment processes.

Generally, the polyethers of PEG will be protonized in an acidic solution, whereas the counter anions adsorbed on the surfaces of elementary particles would react with the protonized PEG through the electrostatic attraction, and it induces that even the elementary particles can be enwrapped and separated, and then stack into looser particles with interparticle pileup pores. And the

electrostatic attraction among the SO_4^{2-} and the protonized PEG would be stronger than that of Cl^- due to its higher charge amount. Thus, the precipitate derived from an $NH_4Al(SO_4)_2$ solution is more stiff than that from an $AlCl_3$ solution as shown in Fig. 2a and c. In the near neutral conditions, PEG molecules adsorbed on the surfaces of aluminum hydrate would limit its growth during the precipitation process [22,24], and then lead to the formation of colloid particles. According to the previous reports, the point of zero charge (PZC) was close to 9.00 for the pseudoboehmite [25,26]. In the present condition, the surface charge is low at pH 7.00–8.00, which is near to the above PZC. Thus, a quick coagulation of the formed colloids would result in the formation of loose particles with relatively large particle size, and large amounts of PEG enfolded in these loose particles lead to the formation of floccus with intraparticle porous structures as shown in Fig. 2b and d. Namely, the acidities of reaction solutions and PEG existing forms have obvious impact on the morphology and structure of precipitate precursors.

3.2. Effects of the reaction conditions on the crystallinities of the products

Fig. 4 depicts the representative XRD patterns of various intermediates derived from $AlCl_3$ and $NH_4Al(SO_4)_2$ solutions. As can be seen from Figs. 4a, b, e and f, the precursors synthesized at different aluminum salt and pH value solutions show amorphous structures, and the intermediates PC2-5 (Fig. 4c) and PC2-7 (Fig. 4d), derived from the azeotropic distillation process, still show amorphous structures no matter what the solution's pH value is. However, the intermediates derived from an $NH_4Al(SO_4)_2$ solution show different crystal phases depending on the pH value of reaction solution. PS2-5 still shows an amorphous structure (Fig. 4g) similar to the PC series of products, while PS2-7 (Fig. 4h) can be ascribed to a pseudoboehmite crystal phase (JPCDS 21-1307) [27–29], indicating that PS1-7 was reconstructed during the distillation process.

Fig. 5 shows the XRD patterns of various calcined products derived from $AlCl_3$ solutions. PC3-5-973 (Fig. 5a) and PC3-7-973 (Fig. 5d) show some weak diffraction peaks of γ-Al_2O_3, indicating that crystallization just begins; whereas PC3-5-1073 (Fig. 5b) and PC3-7-1073 (Fig. 5e) show obvious diffraction peaks of γ-Al_2O_3, indicating that the amorphous precursors have almost transformed into γ-Al_2O_3, the intensities of diffraction peaks of PC3-5-1173 (Fig. 5c) and PC3-7-1173 (Fig. 5f) increase slightly with enhancing the calcinations temperature to 1173 K. The XRD patterns of various calcined products derived from $NH_4Al(SO_4)_2$ solutions are depicted in Fig. 6. Only amorphous structures could be observed in PS3-5-973 (Fig. 6a) and PS3-5-1073 (Fig. 6b), and γ-Al_2O_3 diffraction peaks appear in the product calcined at 1173 K (Fig. 6c); while the intermediate PS2-7 shows a phase transformation course similar to the PC series of an intermediate as shown in Fig. 6d–f. Namely, the intermediates PC2-5, PC2-7 and PS2-7 tend to transform into γ-Al_2O_3 more easily in comparison to PS2-5.

Above results indicate that crystal phases for PC1-5, PC1-7 and PS1-5 almost remain unchanged during the distillation process, and PS1-7 transforms from amorphous to pseudoboehmite

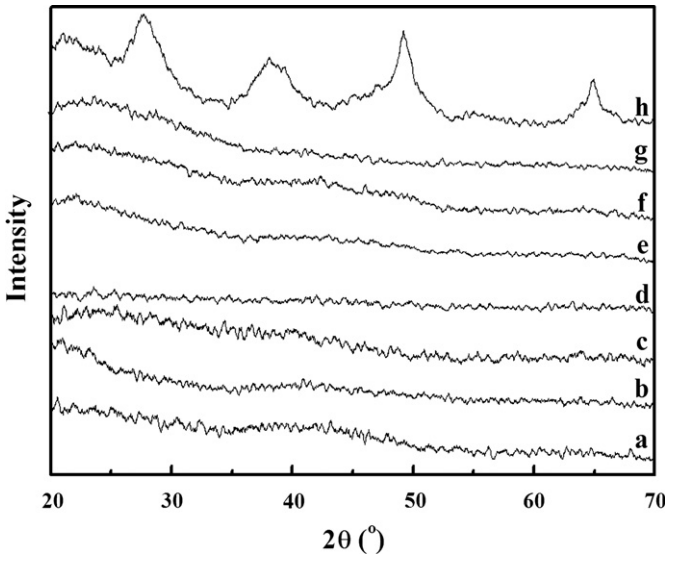

Fig. 4. XRD patterns of various precursors and refluxed products derived from an $AlCl_3$ and an $NH_4Al(SO_4)_2$ solution with different acidities: (a) PC1-5, (b) PC1-7, (c) PC2-5, (d) PC2-7, (e) PS1-5, (f) PS1-7, (g) PS2-5 and (h) PS2-7.

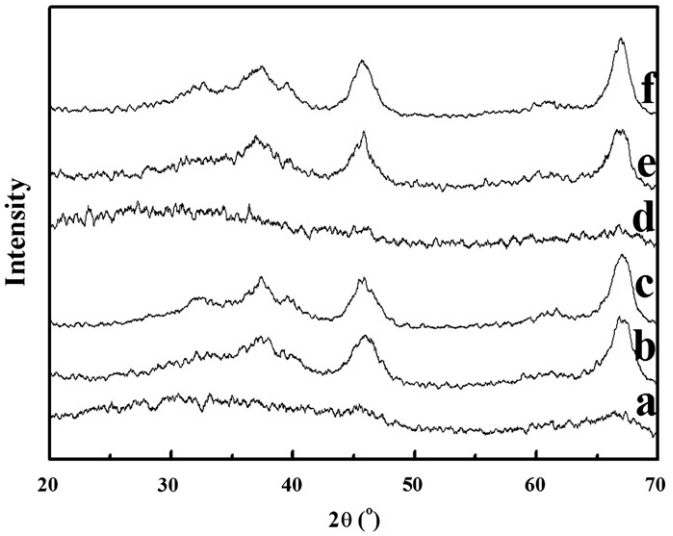

Fig. 5. XRD patterns of precursors and calcined products derived from an $AlCl_3$ solution with different acidities: (a) PC3-5-973, (b) PC3-5-1073, (c) PC3-5-1173, (d) PC3-7-973, (e) PC3-7-1073 and (f) PC3-7-1173.

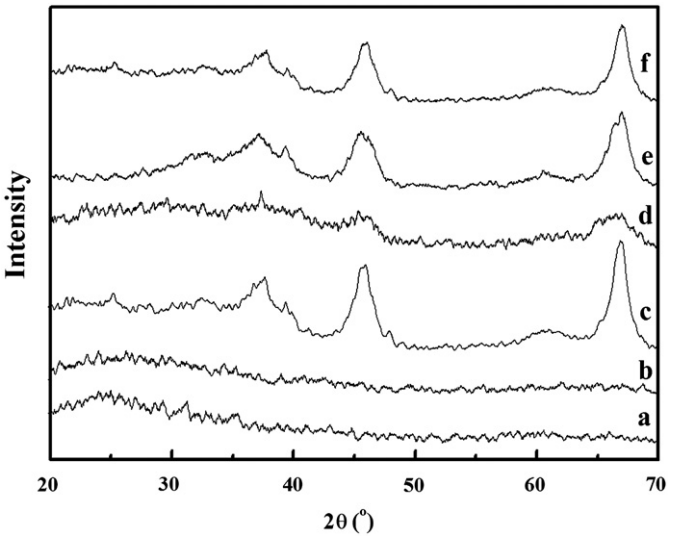

Fig. 6. XRD patterns of precursors and calcined products derived from a $NH_4Al(SO_4)_2$ solutions with different acidities: (a) PS3-5-973, (b) PS3-5-1073, (c) PS3-5-1173, (d) PS3-7-973, (e) PS3-7-1073 and (f) PS3-7-1173.

combining with dissolution and recrystallization processes [22]; whereas PC2-5, PC2-7 and PS2-7 tend to transform into γ-Al_2O_3 more easily in comparison to PS2-5. Considering that PS2-5 is a stable compact aggregation, and the other three intermediates have loose floccules or lamellar structures as observed from TEM images of the refluxed products (Fig. 3), it can be concluded that a looser structure of PC2-5, PC2-7 and PS2-7 have lower activation energy, and then lead it to more easily transforming into γ-Al_2O_3 in comparison with PS2-5.

3.3. Effects of the reaction conditions on the microstructures of the products

Mesoporous structures of the above alumina materials are confirmed by an N_2 adsorption–desorption isotherms (Figs. 7 and 8). The corresponding pore parameters of various calcined aluminas derived from different conditions are summarized in Table 1. According to the original IUPAC classification [30], isotherms for these alumina materials show shapes similar to type IV isotherms. Hysteresis loops arise at middle- and near-saturation vapor pressure stages, representing the existence of mesopores, and N_2 adsorption in low relative pressure indicates the unsaturated adsorption of monomolecule on the mesoporous walls.

For the products PC3-5, PC3-7 and PS3-5 calcined at different temperatures, the adsorption isotherms raise abruptly with increasing the relative pressure due to the capillary condensation in the mesopores. The jumps of N_2 adsorption branches in high relative pressure regions for the three kinds of products could be attributed to the condensation of N_2 in the pores among the big particles and frameworks [31]. Moreover the adsorption–desorption isotherms of above three types of materials can be attributed to a mixed types of H1 and H2 hysteresis loops, while the PS3-7 series products show H3 type hysteresis loops with the jumps in the N_2 adsorption isotherms starting at higher relative

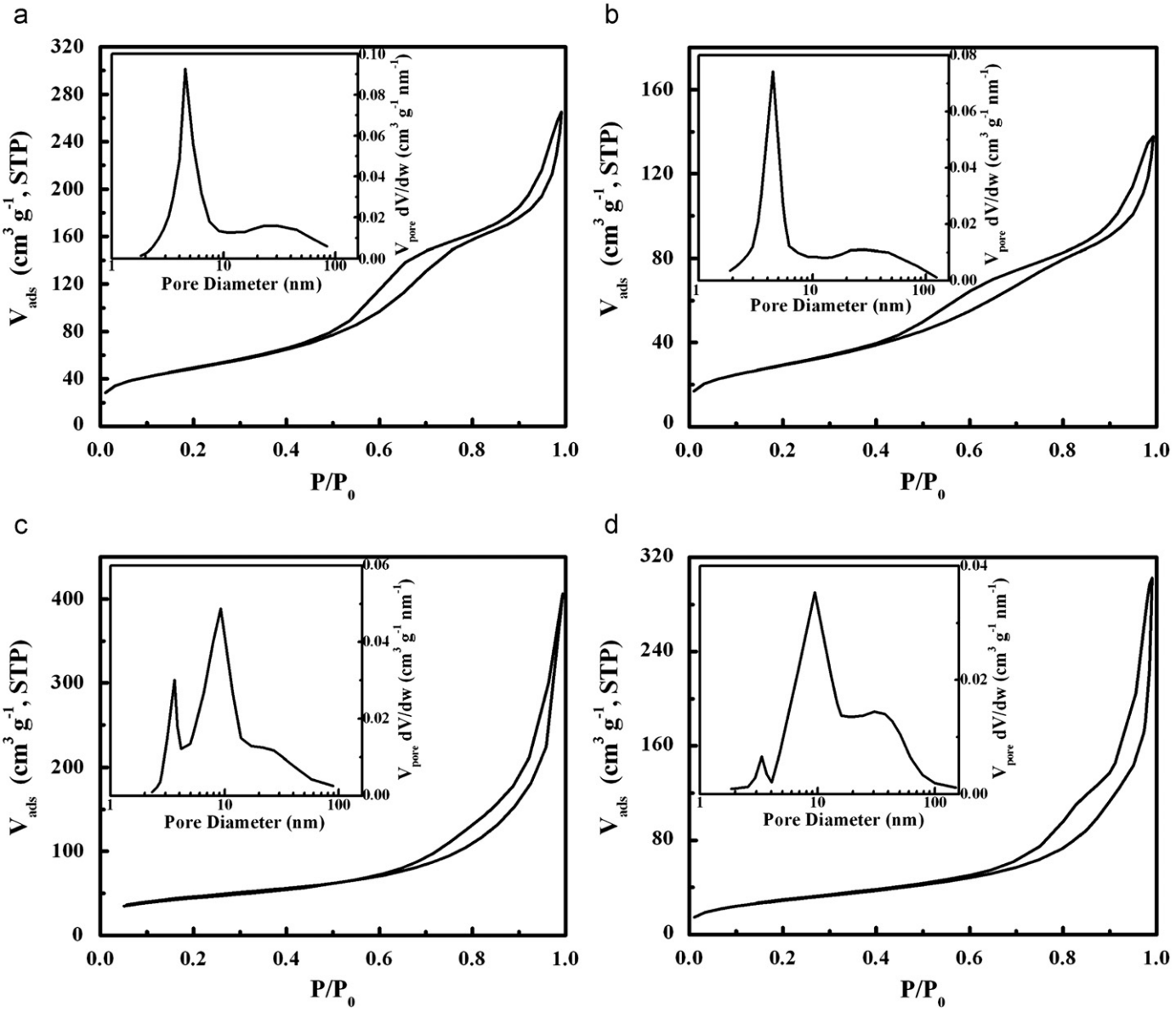

Fig. 7. Nitrogen adsorption/desorption isotherms and BJH pore size distributions (inset) for various calcined products derived from an $AlCl_3$ solution with different acidities: (a) PC3-5-1073, (b) PC3-5-1173, (c) PC3-7-1073 and (d) PC3-7-1173.

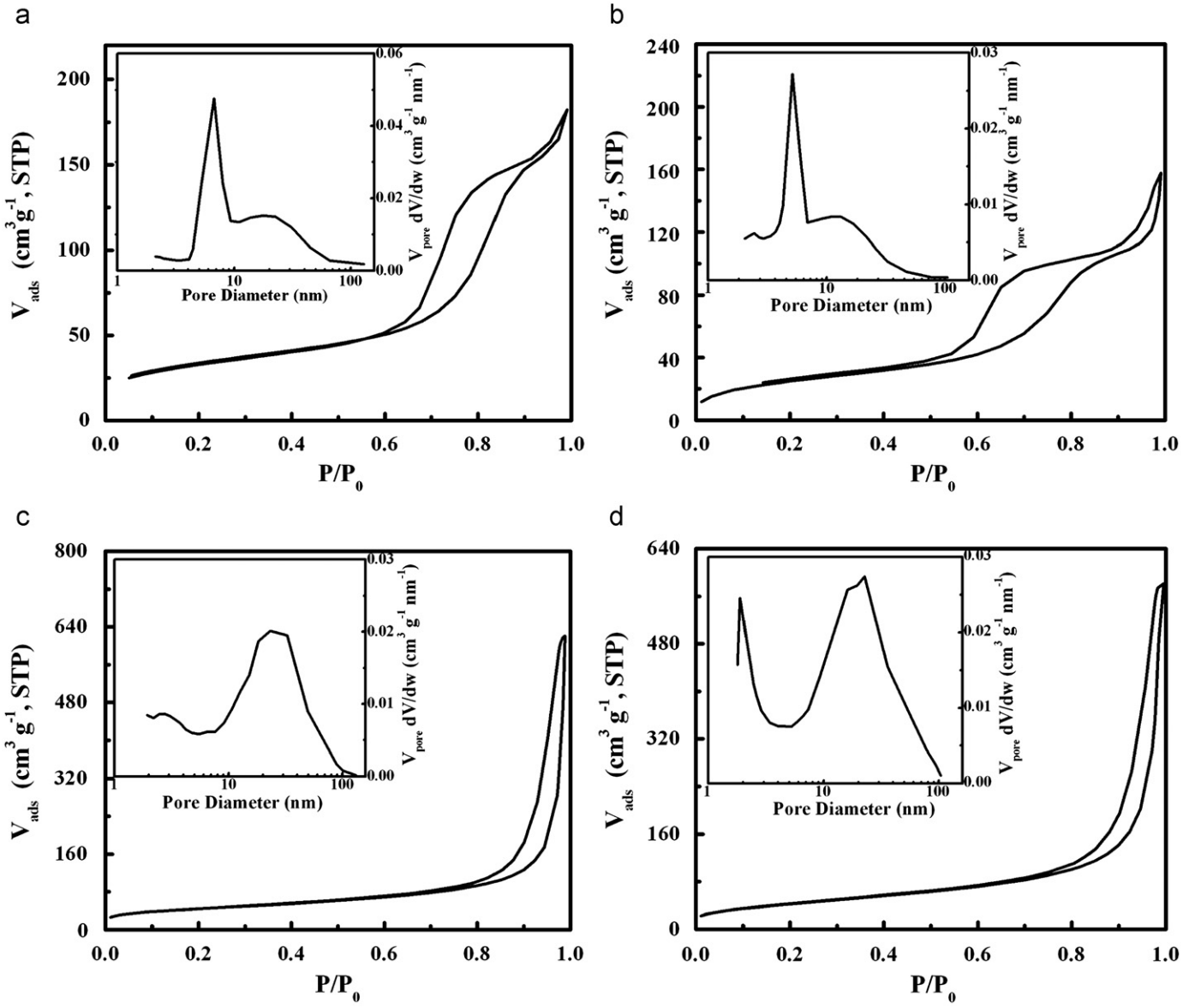

Fig. 8. Nitrogen adsorption/desorption isotherms and BJH pore size distributions (inset) for various calcined products derived from $NH_4Al(SO_4)_2$ solutions with different acidities: (a) PS3-5-1073, (b) PS3-5-1173, (c) PS3-7-1073 and (d) PS3-7-1173.

Table 1
Textural properties of various calcined alumina nanomaterials.

Samples	S_{BET} ($m^2 g^{-1}$)	Mean pore size[a] (nm)	Pore volume[b] ($cm^3 g^{-1}$)
PC3-5-1073	177	7.2	0.410
PC3-5-1173	105	6.7	0.213
PC3-7-1073	158	15.9	0.629
PC3-7-1173	106	15.1	0.468
PS3-5-1073	117	8.7	0.282
PS3-5-1173	93	7.7	0.244
PS3-7-1073	157	23.5	0.961
PS3-7-1173	156	19.2	0.899

[a] Average pore diameter calculated from BJH desorption average pore width (4V/A).
[b] Single point total pore volume at the relative pressure of ca. 0.995.

pressure regions (P/P_0=0.65), which can attribute to the inter-crystallites voids among those stacked nanofibers.

The BJH pore size distributions of various products are also depicted in the insets of Figs. 7 and 8. Generally, pore sizes can be determined by the jump position of middle relative pressure regions. As for the PC series of products, PC3-5-1073 and PC3-5-1173 show jump positions at relative pressures (P/P_0) in the range 0.36–0.39, while PC3-7-1073 and PC3-7-1173 start at 0.57–0.58, this indicates that the pore size distributions of PC3-5 series of calcined products are narrower than those of the PC3-7 series of calcined products. It is coherent with TEM observations in Fig. 1 and the pore size distributions in Fig. 7a–d. As for the PS series of products, PS3-5-1073 and PS3-5-1173 have narrow pore size distributions, it is consistent with the existing intraparticle pores as an observation from Fig. 1c, while the PS3-7 series products have widest pore size distributions among all four series of products because of the irregular shapes and sizes of pores derived from an accumulation of nanofibers [32]. Moreover the bimodal pore size distributions for the obtained alumina particles in Figs. 7 and 8 further validate the observations on the coexistence of intraparticle and interparticle porous structures, especially for the PC3-5, PC3-7 and PS3-7 series of calcined product as shown in Fig. 1.

As can be seen from Table 1, porous alumina (PC3-5-1073 and PC3-5-1173) derived from the acidic $AlCl_3$ solution have smaller mean pore sizes (7.2 and 6.7 nm), in comparison with those (15.9 and 15.1 nm) of products, (PC3-7-1073 and PC3-7-1173) derived from the near neutral solution. It is coherent with above analysis on the adsorption–desorption isotherms. The mean pore sizes (8.7 and 7.7 nm) of porous materials prepared with $NH_4Al(SO_4)_2$ in the acidic solution are far smaller than those (23.5 and 19.2 nm) prepared in the neutral solution, and the pores are derived from an accumulation among nanofibers. Alumina products with crystallized porous walls prevail over the amorphous alumina in the industrial application because porous materials are usually used in high temperature condition, where an excellent thermal stability is indispensable. Nearly, all materials have more than $100\,m^2\,g^{-1}$ specific surface areas even after calcinations at 1173 K. It is worth noting that BET surface area of PS3-7 nearly has no change when calcinations temperature is enhanced from 1073 to 1173 K, indicating the good thermal stability of this kind of nanofibrous structure, which is beneficial for enlarging its application field.

It has been reported that the pseudoboehmite could directly form from aluminum hydroxide at about 373 K [33]. The present distillation temperature (390 K) is similar to the high temperature surrounding of previous literatures to some extent [27,34,35]. Therefore, the amorphous precipitate PS1-7 (Fig. 2d) derived from the neutral reaction solution can transform into 2-D pseudoboehmite lamella (Fig. 3d) through the azeotropic distillation process, and then into 1-D γ-alumina nanofibers (Fig. 1d) after calcinations, this is in consistence with the previous literatures [27,34–37]. The crystal phase and morphology transformations can only be observed in the situation of an $NH_4Al(SO_4)_2$ solution with near neutral condition, whereas PS1-5 derived from the acidic reaction solution shows completely different phenomena as shown in Fig. 2c. It can be ascribed to the enwrapping function of PEG under the acidic reaction conditions, which then transform into more compact aggregation as shown in Fig. 3c, but not a lamellar pseudoboehmite during the following distillation process. Those compact aggregations contain large amount PEG, and porous structures (Fig. 1c) can be obtained after calcinations due to the burning out of PEG. Namely, the reaction conditions lead to those morphological differences existing among the precipitates and their calcined products.

In the present experiments, it also shows that the formation of lamellar pseudoboehmite depends on the counter anions of aluminum salt. As mentioned above, the loose particles derived from the neutral solution would be beneficial for the reconstruction during the distillation process, and SO_4^{2-} can influence the reconstruction due to its higher charge amount. The amorphous precipitate would experience nucleation and growth during the reconstruction process. Residual SO_4^{2-} would re-adsorb on the surfaces of aluminum hydroxide, and the selective adsorption of SO_4^{2-} on some surfaces of aluminum hydroxide can reduce the binding energy of these crystal faces, and retard their growth. Thus, the selective adsorption of inorganic anions combined with distillation process would change the morphology and crystal phase of an amorphous precipitate, and then lead to the lamellar pseudoboehmite as shown in Fig. 3d. It was found that Cl^-, however, could obviously block the formation of lamellar pseudoboehmite during the distillation process. Probably, Cl^- could adsorb on the particle surfaces equally and dynamically, which is different from the situation of SO_4^{2-}. Therefore, the growth of all particle surfaces would behave isotropy, and then the preferential growth of pseduoboehmite is restrained during the distillation process. The structure of intermediate after a distillation process is still amorphous (Fig. 4d), indicating the suppression effect of Cl^- on the crystal phase transformation. However, the differences in morphology between the refluxed intermediate (Fig. 3d) and the precipitate (Fig. 2d) indicated that the distillation process still has an effect on the transformation of precursor. On the bases of the above discussion, the textural evolutions of the present porous alumina materials can be attributed to the different reaction conditions, which lead to the differences in the morphologies and microstructures of the precipitates, intermediates and their calcined products.

4. Conclusion

Mesoporous γ-alumina particles can be synthesized by a traditional precipitation method using inorganic salts as an aluminum source combined with heterogeneous azeotropic distillation and calcination processes. Effects of the aluminum salt counter ion, pH value, surfactant PEG and the distillation process on the structural or textural evolution of alumina particles were investigated. The differences in the product morphologies are related to counter anions and the existing form of PEG molecule in the reaction solutions with different acidities. The experimental results show that amorphous precipitate obtained from a neutral solution are looser than that derived from an acidic solution, and the effect of Cl^- on the morphology of material is different from SO_4^{2-}. The existence of Cl^- would result in alumina particles with porous structure, and pileup pores can be obtained from an acidic reaction solution, while intraparticle pores from a near neutral reaction solution. Nearly, all these materials have more than $100\,m^2\,g^{-1}$ specific surface areas. The present method might offer an effective approach to create new porous alumina nanomaterials from an aqueous media, and has promising industrial application due to its inexpensive and facile process.

Acknowledgments

This work is supported by the Natural Science Foundation of China (20871096), Program for New Century Excellent Talents in University (NCET-07-0637), and the Important Item Nano-Specialized Foundation (2005AA105A01) of Hubei Province, China.

References

[1] C.T. Kresge, M.E. Leonowicz, W.J. Roth, J.C. Vartuli, J.S. Beck, Nature 359 (1992) 710–712.
[2] J.S. Beck, J.C. Vartuli, W.J. Roth, M.E. Leonowicz, C.T. Kresge, K.D. Schmitt, D.H. Olson, E.W. Sheppard, S.B. McCullen, J.B. Higgins, J.L. Schlenker, J. Am. Chem. Soc. 114 (1992) 10834–10843.
[3] P. Behrens, Adv. Mater. 5 (1993) 127–132.
[4] M.E. Davis, Nature 364 (1993) 391.
[5] J.M. Thomas, Nature 368 (1994) 289.
[6] J. Cejka, Appl. Catal. A: Gen. 254 (2003) 327–338.
[7] F. Vaudry, S. Khodabandeh, M.E. Davis, Chem. Mater. 8 (1996) 1451–1464.
[8] J. Cejka, N. Zilkova, J. Rathousky, A. Zukal, Phys. Chem. Chem. Phys. 3 (2001) 5076–5081.
[9] S.A. Bagshaw, T.J. Pinnavaia, Angew. Chem. Int. Ed. Engl. 35 (1996) 1102–1105.
[10] S. Cabrera, J.E. Haskouri, J. Alamo, A. Beltran, D. Beltran, S. Mendioroz, M.D. Marcos, P. Amoros, Adv. Mater. 11 (1999) 379–381.
[11] V. Gonzalez-Pena, I. Diaz, C. Marquez-Alvarez, E. Sastre, J. Perez-Pariente, Micropor. Mesopor. Mater. 44–45 (2001) 203–210.
[12] Q. Liu, A.Q. Wang, X.D. Wang, T. Zhang, Micropor. Mesopor. Mater. 92 (2006) 10–21.
[13] Z.H. Gan, G.L. Ning, Y. Lin, Y. Cong, Mater. Lett. 61 (2007) 3758–3761.
[14] Q.S. Huo, D.I. Margolese, U. Ciesla, D.G. Demuth, P.Y. Feng, T.E. Gier, P. Sieger, A. Firouzi, B.F. Chmelka, F. Schuth, G.D. Stucky, Chem. Mater. 6 (1994) 1176–1191.
[15] R.H. Zhao, F. Guo, Y.Q. Hu, H.Q. Zhao, Micropor. Mesopor. Mater. 93 (2006) 212–216.
[16] P. Bai, W. Xing, Z.X. Zhang, Z.F. Yan, Mater. Lett. 59 (2005) 3128–3131.
[17] J.F. Poco, J.H. Satcher Jr., L.W. Hrubesh, J. Non-Cryst. Solids 285 (2001) 57–63.

[18] J. Walendziewski, M. Stolarski, M. Steininger, B. Pniak, React. Kinet. Catal. L. 66 (1999) 71–77.
[19] E. Elaloui, A.C. Pierre, G.M. Pajonk, J. Catal. 166 (1997) 340–346.
[20] T.B. Du, S.M. Jang, B.W. Chen, Chem. Eng. Sci. 62 (2007) 4864–4868.
[21] H.S. Potdar, K.W. Jun, J.W. Bae, S.M. Kim, Y.J. Lee, Appl. Catal. A: Gen. 321 (2007) 109–116.
[22] X. Liu, Z.G. Wu, T.Y. Peng, P. Cai, H.J. Lv, W.L. Lian, Mater. Res. Bull. 44 (2009) 160–167.
[23] K. Kandori, S.P. Ohnishia, M. Fukusumi, Y. Morisada, Colloids Surf. A: Physicochem. Eng. Aspects 331 (2008) 232–238.
[24] X. Zhang, Y. Zhao, C.B. Zhang, Chin. J. Chem. Phys. 17 (2004) 614–617.
[25] D. Fauchadour, F. Kolenda, L. Rouleau, L. Barre, L. Normand, Stud. Surf. Sci. Catal. 143 (2002) 453–461.
[26] C.R. Evanko, R.F. Delisio, D.A. Dzombak, J.W. Novak Jr., Colloids Surf. A: Physicochem. Eng. Aspects 125 (1997) 95–107.
[27] Y.Y. Li, J.P. Liu, Z.J. Jia, Mater. Lett. 60 (2006) 3586–3590.
[28] M. Inoue, M. Kimura, T. Inui, Chem. Mater. 12 (2000) 55–61.
[29] S. Rana, S. Ram, J. Solid State Chem. 157 (2001) 40–49.
[30] K.M.S. Khalil, J. Colloid Interf. Sci. 307 (2007) 172–180.
[31] Y. Luo, G.Z. Lu, J.Z. Huang, Y.L. Guo, J.S. Wang, J East China Univ. Sci. Technol. 29 (1) (2003) 38–42.
[32] H.Y. Zhu, J.D. Riches, J.C. Barry, Chem. Mater. 14 (2002) 2086–2093.
[33] C. Misra, Industrial alumina chemicals. ACS Monogr, vol. 184, ACS, Washington DC, 1986.
[34] S.C. Kuiry, E. Megen, S.D. Patil, S.A. Deshpande, S. Seal, J. Phys. Chem. B 109 (2005) 3868–3872.
[35] D.B. Kuang, Y.P. Fang, H.Q. Liu, C. Frommen, D. Fenske, J. Mater. Chem. 13 (2003) 660–662.
[36] K.M.S. Khalil, J. Catal. 178 (1998) 198–206.
[37] S.J. Wilson, M.H. Stacey, J. Colloid Interface Sci. 82 (1981) 507–517.